Low-Elevation Ionosphere Spatial Anomalies Discovered from the 20 November 2003 Storm

Godwin Zhang, Jiyun Lee, Seebany Datta-Barua, Sam Pullen, and Per Enge, *Stanford University*

ABSTRACT

This paper presents data from low-elevation satellites on 20 November 2003 in the Ohio region, the area of the largest validated gradients seen to date. As viewed by multiple CORS stations in central and northeastern Ohio, SVN 26 came into view around 2030 UT on this day, rose to an elevation angle of about 15 degrees just after 2100 UT, and set between 2135 and 2200 UT. This observation window is very close to the time that peak ionosphere gradients were observed at those stations on higher-elevation satellites. An ionosphere gradient of about 300 mm/km was discovered on SVN 26 between CORS stations KNTN and SIDN at 2050 UT, when SVN 26 was at about 12.6° elevation relative to these two sites. Thirty minutes later, at 2120 UT, a gradient of about 360 mm/km was discovered between CORS stations GARF and WOOS, when SVN 26 was at about 12.0° elevation. Gradients between 200-300 mm/km were also discovered at other station pairs between 2100 and 2130 UT. Spatial gradients to another low elevation satellite with a similar azimuth angle, SVN 29, were observed to be about 100 –150 mm/km. While comparison of the L1-L2 ionosphere estimates with L1 code-minus-carrier measurements is hindered by higher noise and loss-of-lock on L2, sufficient similarity between the two sets of ionosphere gradient estimates exists to allow us to state that at least some of these observations, including the two largest-gradient cases, can be declared "validated" based on the preponderance of the evidence.

This paper details our recent study of low-elevation satellite observations from the 20 November 2003 ionosphere storm and shows how we arrived at the ionosphere gradient estimates cited above. These newfound observations imply that the means by which the Local Area Augmentation System (LAAS) mitigates anomalous ionosphere spatial gradients may need to be revised.

1.0 INTRODUCTION

As reported in [1,2,3], previous Stanford research has identified the potential for severe ionosphere spatial gradients to affect Local Area Augmentation System (LAAS) integrity. A detailed method for deriving the ionosphere threat model parameter bounds (assuming a constant linear ionosphere gradient "wave front" moving at constant speed with respect to the ground) from recorded CORS data [4] from the ionosphere storms of 6 - 7 April 2000, 29 - 31 October 2003, and 20 November 2003 was developed in this research. The resulting threat model has been used to derive σ_{pr_gnd} and σ_{vig} inflation factors that would sufficiently protect CAT I LAAS user integrity in the presence of this threat model [5]. During these same storms WAAS user integrity was maintained by broadcasting GIVEs high enough to limit precision navigation service for the day [6].

While the additional noise and more frequent loss-of-lock on CORS measurements at low-satellite elevation angles meant that far fewer verifiable anomalies existed for satellites below 12 degrees in previous work, the ones that were present suggested that anomalous gradients in this region, of magnitudes of around 100 to 150 mm/km, were much smaller than for high-elevation satellites. This conclusion was supported by a Honeywell study of anomalous gradients from WAAS "supertruth" data for the October and November 2003 ionosphere storms.

In addition, a hypothesis has been advanced within the community of ionosphere scientists that electron density enhancements were driven by storms in which ionosphere delay increased at higher altitudes within the ionosphere (instead of being concentrated in the region between 250 and 600 km, as assumed by the 2-D ionosphere "shell" model that works well under nominal ionosphere conditions). If this were the case, signals from GPS satellites at low elevations would be likely to "pass under" the bulk of the enhanced ionosphere gradient and thus be relatively unaffected. However, this hypothesis of the vertical concentration of ionosphere anomalies is far from validated – these events are still not well understood in detail by ionosphere theorists.

2.0 DATA AND ANALYSIS PROCEDURE

On 20 November 2003, a coronal mass ejection (CME) from the Sun triggered one of the most severe ionospheric

storms of the past solar cycle. This led to a great storm-enhanced density (SED) in the American sector during the local afternoon. Such an SED was shown to feed a plasmaspheric plume that appeared as a filament structure over the United States [7], as shown in the map of equivalent vertical delays in Figure 1. Dual-frequency GPS slant measurements of the refractive delay of the L1 signal from multiple stations on the ground are plotted on the map at the points, known as the ionospheric pierce point (IPP), at which each line of sight reaches an altitude of 450 km. The IPPs are assigned a color associated with their equivalent vertical delays, converted from slant assuming an ionosphere height of 450 km. The colors on the map are then bi-linearly interpolated between each set of three nearest IPPs. The Continuously Operating Reference Stations (CORS) and International GNSS Service (IGS) networks provide a dense set of measurements of the delays due to electrons in the ionosphere every 30 seconds. They were collected and post-processed in a system described by Komjathy [8] at Jet Propulsion Laboratory in order to detect cycle slips, estimate the satellite and receiver biases, and remove the integer ambiguities. Within this data set we identify candidate high gradients at low elevation that may occur.

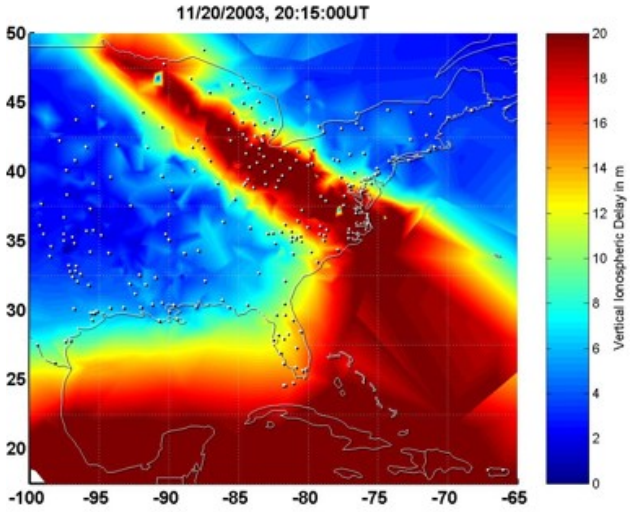

Figure 1: Map of equivalent vertical delays over the eastern U.S. on 20 November 2003 20:15 UT, from 0 m (blue) to 20 m (red), as measured by CORS and IGS stations, shown as shadowed white dots.

The procedure for processing CORS receiver data, identifying anomalies, validating that the anomalies are due to ionosphere events, and estimating gradients is shown in Figure 2. The starting point is "raw" L1 and L2 measurements from selected groups of CORS stations. As mentioned earlier, post-processing of CORS measurements was done by JPL to remove obvious receiver glitches and to correct for satellite and receiver inter-frequency biases. Using this JPL post-processed data, spatial gradients were estimated simply by dividing the difference in slant (not zenith) ionosphere delay between two stations by the ground distance between those two stations, and the results were expressed in terms of mm/km. Stations and times with apparently severe gradients were output to automated screening algorithms that attempt to remove receiver glitches or data outages from consideration (see [5]). However, no automated screening algorithm is perfect. Thus, it was necessary to consult the raw CORS data to determine what actually happened and to make a "manual" (i.e., person-made) judgment.

Dual-frequency data are prone to L2 (semi-codeless) loss of lock, particularly for satellites at low elevation angles. Therefore, once a possible observation of an anomalous gradient is identified, we compare the dual-frequency observation with the observation based on only the L1 frequency code-carrier divergence. This L1-only measurement is more robust to outages and cycle slips. If both the dual-frequency and single-frequency observations are in agreement, the gradient is declared to be "validated." The processing methodology is described in greater detail in [3]. It is the final manual comparison and verification that makes finding and validating extreme ionosphere gradients a time-consuming process.

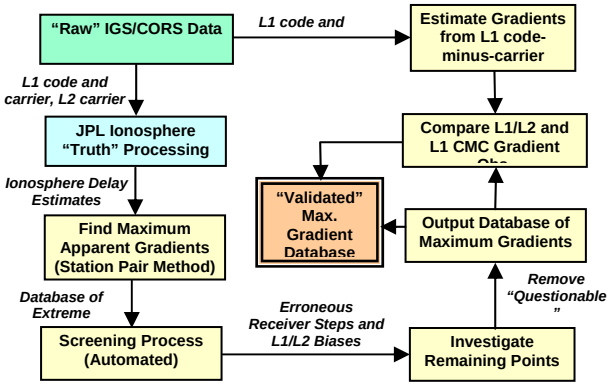

Figure 2: Ionosphere Anomaly Data Analysis Procedure.

3.0 RESULTS

LAAS provides precision navigation approach service to users within tens of kilometers of the LAAS Ground Facility (LGF), which includes multiple reference receivers to generate GPS corrections and a VHF Data Broadcast (VDB) to transmit these corrections to nearby users. To identify spatial gradients in the ionosphere that are possible over baselines of similar length, we look to geographic regions where stations are at the highest density, namely Ohio. The Ohio Department of

Transportation has installed a large number of Trimble 5700 receivers and Trimble L1/L2 choke ring antennas throughout the state and made these available as part of the CORS network. The location of these stations observing satellite (SVN) 26 from 2000 – 2100 UT is shown on the map plotted in Figure 3.

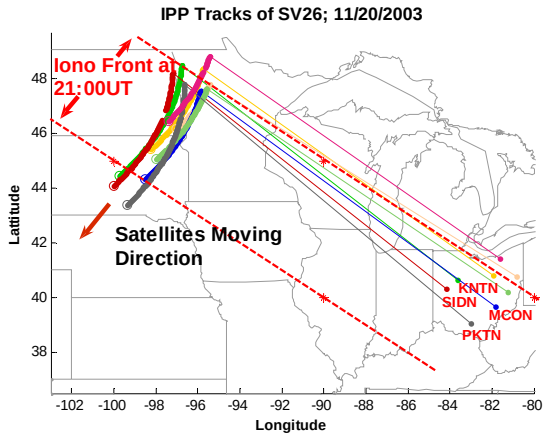

Figure 3: Map of CORS stations and the azimuthal direction at which SVN 26 is viewed. Arcs indicate the position of the ionosphere pierce points (IPPs) from 20:30 – 21:30 UT.

In Figure 3, the receivers in Ohio are identified with filled circles. Arcs identify the points at which the lines of sight from the stations to SVN 26 reach an altitude of 350 km (the assumed ionosphere pierce point, or IPP), from 2030-2130 UT. Lines point from each of these stations to the IPP at which SVN 26 is viewed at 2030 UT. Notice that the azimuthal viewing direction is similar to the orientation of the plume shown in Figure 1. For this reason, we expect pairs of stations whose lines of sight straddle the red-colored filament of enhanced delay to exhibit particularly high gradients. Two pairs of stations that we analyze more closely are identified on the map: KNTN/SIDN and MCON/PKTN.

Figure 4(a) shows the dual-frequency measurements of delay at L1 in meters made from CORS stations KNTN and SIDN to SVN 26 as a function of time in decimal hours. KNTN begins with a slant delay of about 28 m and just before 2100 UT appears to rise to nearly 40 m. Meanwhile SIDN has 40-meter delays at 2040 UT that gradually drop to 25 m by 2130 UT. By dividing the difference in the apparent delay by their separation distance of 59 km, we compute the apparent gradient between the stations, as shown in Figure 4(b). Note that this reaches a maximum absolute value of 350 mm/km. The elevation angle of SVN 26 in degrees from KNTN in Figure 4(c) is shown as a series of red circles. From SIDN, it is shown as a set of green circles. From both stations (SIDN being slightly higher), this elevation angle reaches a peak of about 13 degrees. However, data outages on SIDN's dual-frequency measurements are visible in Figure 4(a), and the jump from 28 m to 35 m on the KNTN (red) curve at 2100 UT calls into question the reliability of the dual-frequency estimate of the slope.

For this reason, as with all other dual-frequency anomaly data, we attempt to "validate" the presence of an actual ionosphere spatial anomaly within this data by returning to the raw L1 measurements and computing half of the code-carrier divergence, which is equal to the ionosphere delay offset by an integer ambiguity. Code-carrier divergence has the advantage of relying on only the L1 frequency, but it contains greater noise than carrier phase L1-L2 data due to the presence of code-phase multipath and the L1 integer ambiguity of the L1 carrier measurement. By manually leveling the L1-only computed slope as a function of time to the dual-frequency slope, we can confirm a maximum slope observed due to this event of 300 mm/km at 2050 UT, as shown in Figure 5.

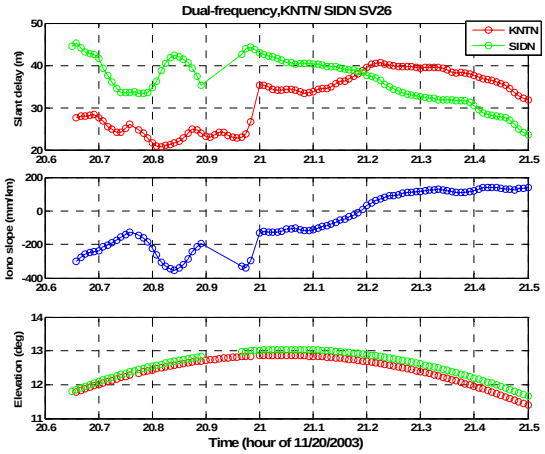

Figure 4: (a) Dual-frequency carrier phase slant measurement of ionosphere delay, in m at L1, for KNTN (red) and SIDN (green); (b) Ionosphere spatial gradient versus time; and (c) Elevation of SVN 26 for KNTN (red) and SIDN (green), as a function of time, in decimal UT hours.

Notice that the data outages present in the slope deduced from the dual-frequency measurements from 2050 to 2100 UT do not exist in the L1-only measurements, confirming that the data gaps are limited to the L2 measurements. The general trend over time between the two slope measurements agrees, including the time during which the L2 data outages occur.

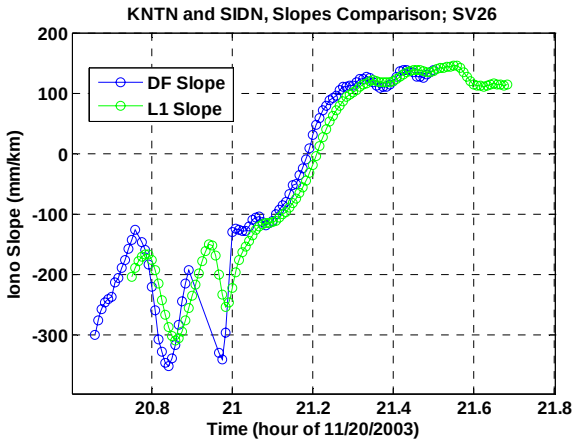

Figure 5: Comparison of dual-frequency (blue) and single-frequency (green) spatial gradient between KNTN and SIDN as a function of time.

To confirm that this observation is not due to bias-leveling errors on receiver data from either KNTN or SIDN, we analyze data from an independent pair of stations also viewing SVN 26. The locations of CORS stations MCON and PKTN in southeastern Ohio are labeled in Figure 3. The JPL-processed dual-frequency measurements of ionosphere delay at L1 from these stations are shown in Figure 6(a) in red (MCON) and green (PKTN) as a function of decimal UT hours. We divide the difference in their ionosphere delays by their 124-km separation distance to compute the ionosphere spatial decorrelation between these stations, as shown in Figure 6(b). The elevation of SVN 26 from MCON (red circles) and PKTN (green circles) is shown to reach a maximum of 11 and 11.5 degrees, respectively, in Figure 6(c).

Dual-frequency data outages are shorter for PKTN compared to KNTN/SIDN, lasting only one or two 30-second epochs each at 2049 and 2100 UT. The data for MCON, though continuous, starts a few minutes later and ends a few minutes earlier than PKTN. The largest slope estimated from the dual-frequency data of this pair of stations occurs at 2050 UT, just after one such data gap. To validate this event and the computed slope value of 300 mm/km, we again turn to the raw CORS data and examine the L1 code-minus-carrier estimate of the ionosphere delay. Since the code-carrier divergence is offset by the integer ambiguity, we manually level it to the dual-frequency computation of slope. The dual-frequency and leveled single-frequency estimate of the spatial gradient are shown in blue and green, respectively, in Figure 7. The blue curve in Figure 7 is the same one plotted in Figure 6(b).

As noted above, the dual-frequency estimate (blue) has gaps at 2049 and 2100 UT due to a lack of dual-frequency data, whereas the single-frequency (green) data are continuous through these periods. In addition, there are single-frequency measurements as early as 2040 UT. One cycle slip on the L1 frequency was identified and manually removed at 2047 UT and is shown as a gap in the single-frequency slope estimate in Figure 7. Despite this one slip, the overall trend between the single- and dual-frequency data agrees quite closely. We validate the maximum estimate slope seen from MCON and PKTN as the largest magnitude slope on the L1-only estimate that has been leveled to the L1-L2 estimate: 250 mm/km at 2050 UT, when SVN 26 was at an elevation angle of about 11 degrees.

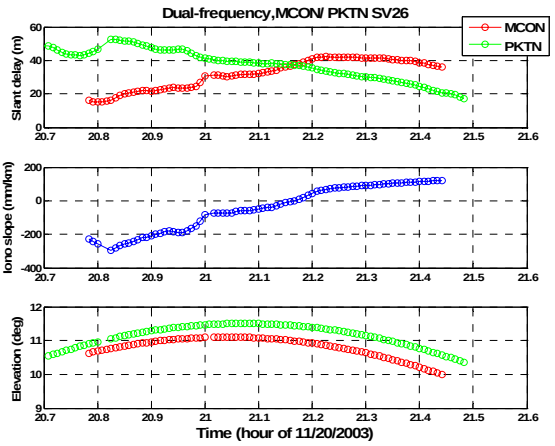

Figure 6: (a) Dual-frequency carrier phase slant measurement of ionosphere delay, in m at L1, for MCON (red) and PKTN (green); (b) Ionosphere spatial gradient versus time; and (c) Elevation of SVN 26 for MCON (red) and PKTN (green), as a function of time, in decimal UT hours.

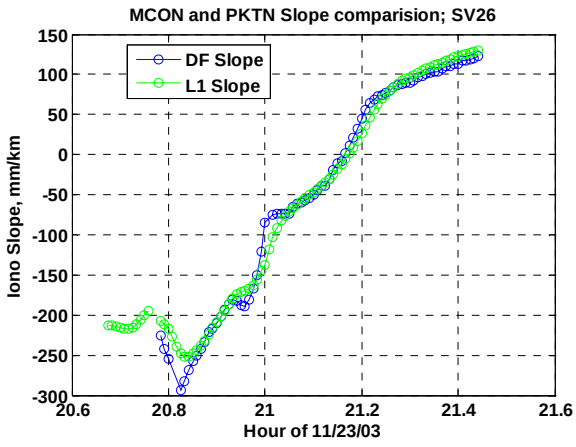

Figure 7: Comparison of dual-frequency (blue) and single-frequency (green) spatial gradient estimates between MCON and PKTN as a function of time.

In addition to those shown in Figure 5 and Figure 7, we have validated ionosphere gradients of 200-300 mm/km from stations in Ohio viewing SVN 26 at about 2050 UT. These observations are summarized on the map in Figure 8 with maximum gradient values in mm/km shown in green and lines connecting the pairs of stations from which the estimates were computed. A dashed red line indicates the position and orientation of the ionosphere anomaly shown in Figure 1 at 2100 UT.

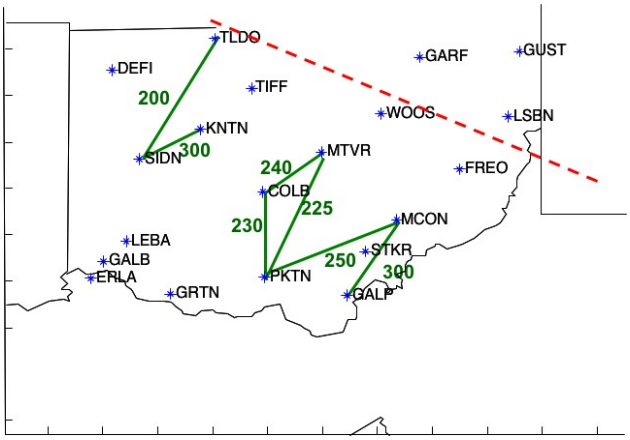

Figure 8: Map of CORS stations in Ohio and ionosphere slopes observed and validated with both dual-frequency and L1-only data from 2045-2050 UT. Solid green lines connect pairs of stations, and validated slope is indicated. Dashed red line marks approximate orientation and position of ionosphere filament edge at 2100 UT.

We also investigate data from a cluster of stations in northeastern Ohio: GARF, GUST, LSBN, FREO, and WOOS. These stations show the largest-magnitude ionosphere gradients that we have validated at 2130 UT. The locations of these stations are shown in Figure 8. Figure 9 is a plot of the dual-frequency measurements of slant ionosphere delay over time from these stations. The three northeastern-most stations are LSBN, GARF, and GUST. The slant delays for these stations remain in the 10 – 15 m range from 2048 – 2015 UT. In contrast, the two stations just to the southwest of the dotted line in Figure 8 begin at 15 m and rise to over 45 m slant delay during the same period as the lines of sight pass through the filament of enhanced ionosphere delay.

The similarity of the trend for FREO and WOOS indicates that this is not a single-receiver failure. The same argument lends confidence to the measurements of LSBN, GARF, and GUST. Individual variations in these stations at the end of the time period are due to differences in station position and elevation angle of SVN 26.

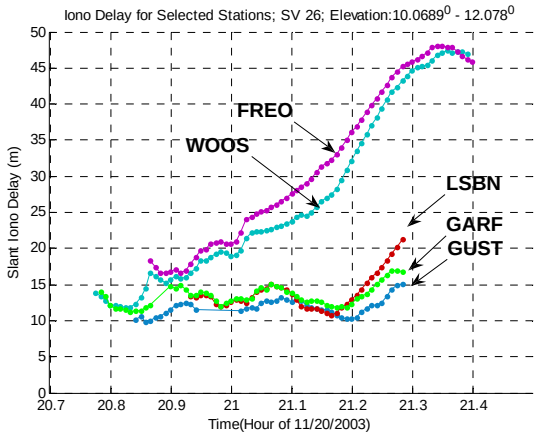

Figure 9: Dual-frequency carrier phase measurements of slant delay in m to SVN 26 as a function of decimal UT hour for CORS stations in Northeastern Ohio.

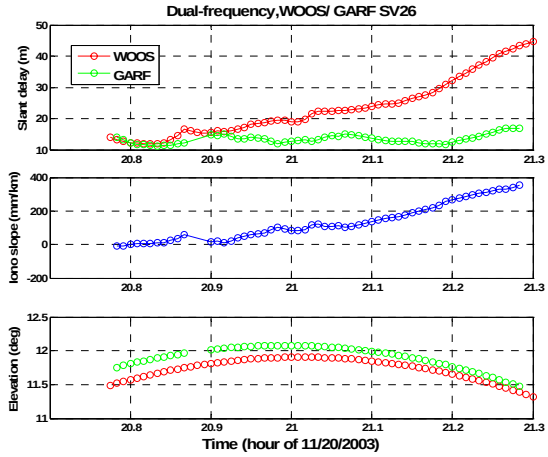

Figure 10: (a) Dual-frequency carrier phase slant measurement of ionosphere delay, in m at L1, for WOOS (red) and GARF (green); (b) Ionosphere spatial gradient versus time; and (c) Elevation of SVN 26 for WOOS (red) and GARF (green), as a function of time, in decimal UT hours.

We analyze one pair of these stations to estimate the ionosphere spatial gradient between them. The station WOOS is just to the southwest of the dotted line; GARF lies 75 km northeast of WOOS. The dual-frequency slant delays for these two stations are re-plotted in Figure 10(a). To estimate the spatial gradient, shown in Figure 10(b), between these two stations, the difference in delay is divided by the station separation distance. The slope rises from 0 mm/km to nearly 400 mm/km as the delay for WOOS rises to 45 m during passage through the anomalous region while GARF holds steady at about 15-18 m. The elevation of SVN 26 from WOOS and GARF are shown as solid blue line and dotted green line, respectively, in Figure 10(c).

As with other dual-frequency measurements we have examined, there is a data gap for GARF at 2054 UT. Unlike the station pairs analyzed above, this is not the time at which the highest gradient is observed to occur between this pair of stations. Instead, the highest slope of more than 350 mm/km occurs at the end of the data track as SVN 26 is setting, at 2117 UT.

To validate this dual-frequency estimate by testing for possible cycle slips on L2, we compare it to the L1-only code-minus-carrier estimate of the ionosphere spatial gradient. The dual-frequency-based slope from Figure 10(b) is re-plotted with connected blue circles in **Error! Reference source not found.**. The single-frequency estimate of the slope is manually leveled to the mean value of the dual-frequency slopes to remove the integer ambiguity, and is shown in green circles connected by a line. There are continuous single-frequency measurements except at one epoch at 2052 UT, at which time the line connecting the L1-only slope is broken. The L1 measurement at this time had a visible cycle slip and was manually removed. Except for this epoch, there are single-frequency data throughout the period during which there are no dual-frequency measurements, between 2052 and 2054 UT. Both dual- and single-frequency measurements are continuous through the remainder of the pass, and both slope estimates show the same rising trend. Based on the agreement between the two and the absence of cycle slips that might introduce errors, we validate the highest slope between the stations WOOS and GARF occurs at 2120 UT and is about 360 mm/km, which is the highest ionosphere spatial gradient we have observed at low elevation.

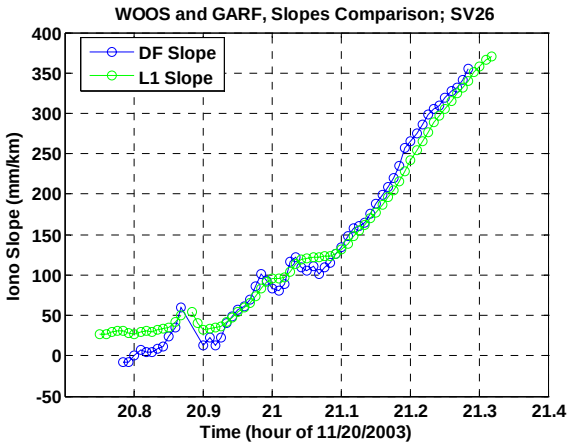

Figure 11: Comparison of dual-frequency (blue) and single-frequency (green) spatial gradient estimates between WOOS and GARF as a function of time.

It is notable that the time at which this largest gradient is measured, 2120 UT, is not long after to the time (around 2100 – 2110 UT) when the highest gradients at higher elevation were observed by [1]. The tables in the appendices to [1] also show that the large gradient between WOOS and GARF on SVN 26 was noticed, but this observation could not be validated as a stand-alone feature at that time and thus was not included in the resulting LAAS ionosphere threat model. The key to validating the SVN-26 results shown in this paper is that similar gradients and patterns of ionosphere delay change over time were seen across Ohio on multiple CORS stations. This was not apparent in [1] because the data were analyzed on a station-pair by station-pair basis, and only the events with little-to-no questionable measurement content (e.g., no L2 measurement outages or cycle slips) were considered to be of "validatable" quality.

All spatial gradients estimated so far have been for lines of sight towards SVN 26. To search for other possible high gradients at low elevation, we consider the elevation angle as a function of time, as shown in Figure 12. Although there are as many as 10-12 satellites visible from this region between 2000 and 2100 UT, to identify the highest spatial gradients, we choose to plot only those whose azimuth angle is aligned within +/– 15 degrees of the orientation of the filament. Based on Figure 1, we compute the azimuth angle of the edge of the anomaly to be 307 degrees, so we plot the elevation of those SVNs whose azimuth is 292 – 322 degrees. Each station in Ohio viewing a given satellite observes it at a slightly different elevation. Thus, plotted together, individual lines to one satellite merge into a single colored region several degrees thick in Figure 12.

The satellite SVN 26 we have analyzed extensively in this paper is between 10-15 degrees from 2030-2130 UT, shown in green. Satellites that were observed by [1] to reveal high ionosphere gradients at higher elevations are SVN 38 (yellow-green) at 1900-2000 UT, and SVN 44 (light purple) at 2000-2100 UT, and SVN 46 (black) from 1930-2030 UT.

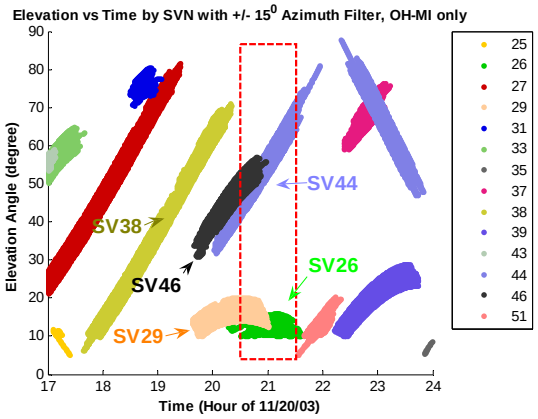

Figure 12: Elevation in degrees as a function of UT hour for satellites whose azimuth angle is 292 – 322 degrees. SVNs are identified in the legend.

During the time in which the anomaly is passing over the Ohio region, there is one satellite in addition to SVN 26 that is at low elevation and oriented almost parallel to the filament edge: SVN 29 (shown as peach-colored in Figure 12). We examine the gradients for this satellite measured from the CORS stations in Ohio. The positions of the CORS stations in Ohio are shown in Figure 13. Line segments point from each CORS station to the IPP for the line of sight to SVN 29 at 2030 UT. This shows that the azimuthal direction is northwest, closely aligned with the boundaries of the anomaly region in Figure 1. Arcs indicate the position of the IPPs from 2030 to 2130 UT as SVN 29 rises and sets. The IPPs move from northeast to southwest over time.

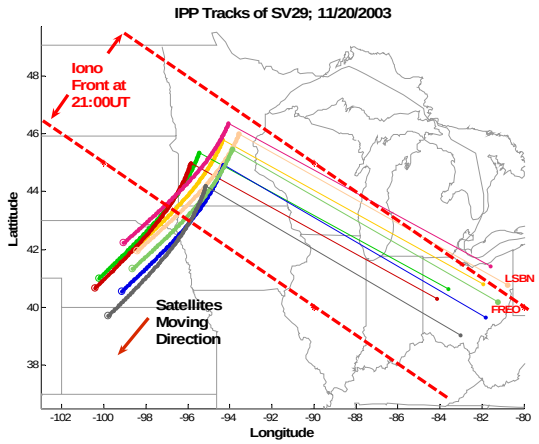

Figure 13: Map of Ohio CORS stations and lines pointing in the azimuthal direction at which SVN 29 is viewed. Arcs indicate the position of the IPPs from 20:30 – 21:30 UT.

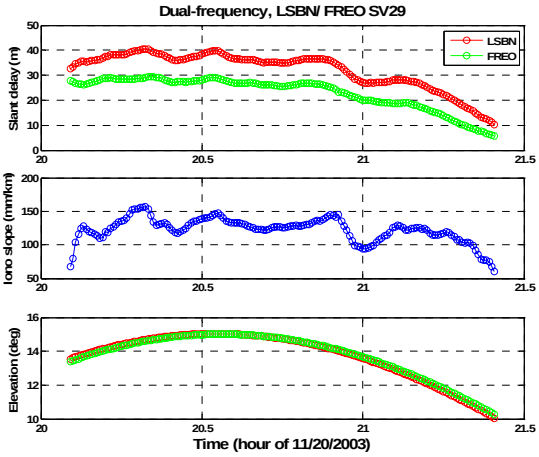

Figure 14: (a) Dual-frequency carrier phase slant measurement of ionosphere delay, in m at L1, for LSBN (red) and FREO (green); (b) Ionosphere spatial gradient versus time; and (c) Elevation of SVN 29 for LSBN (red) and FREO (green), as a function of time, in decimal UT hours.

In Figure 14, we illustrate the dual-frequency ionosphere spatial gradient observed to SVN 29 from stations LSBN and FREO labeled on Figure 13. Figure 14(a) is a plot of the slant delays as a function of UT hour for LSBN (red) and FREO (green). In this case, the dual-frequency data are continuous for the entire period. The trend is very similar for both, but the delays are about 9 m larger for LSBN and FREO. This difference in delay results in a slope over time, in Figure 14(b), of between 100 and 150 mm/km when divided by the station separation distance of 73 km. The elevation of SVN 29 viewed from these two stations, shown in Figure 14(c), ranges from 10 – 15 degrees for both LSBN (solid blue line) and FREO (dotted green line).

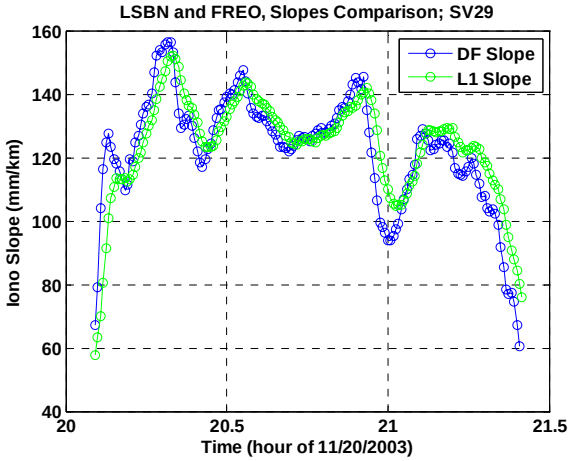

Figure 15: Comparison of dual-frequency (blue) and single-frequency (green) spatial gradient estimates between LSBN and FREO as a function of time.

Although there are no data gaps in the dual-frequency data, we again compare the slope to a single-frequency slope that is derived from the L1 code-carrier divergence, as is our normal validation practice in every case. The slope over time shown in Figure 14(c) is re-plotted in blue on Figure 15. The L1-only measurement of the slope is leveled to this curve to remove the integer ambiguity and is plotted in green. Both the single- and dual-frequency estimated slopes have a very similar trend over time, which lends credence to the slope values measured.

One thing to note in Figure 15 is that the maximum ionosphere spatial gradient between LSBN and FREO as they view SVN 29 is only about 150 mm/km. While still anomalously high, this is less than half the magnitude of the largest slopes estimated from northeastern Ohio to SVN 26. Analysis of the spatial gradient between WOOS and GARF (not shown) in northeast Ohio yields slopes comparable to 150 mm/km. The observation of 150 mm/km slopes only 30 minutes earlier and at an azimuth direction only a few degrees different from the lines of

sight to SVN 26 illustrates the challenging nature of this search process in identifying maximum spatial gradients in this dataset. The confluence of several factors – extremely anomalous ionosphere behavior, dense stations, a satellite at just the right viewing angle at the time the anomaly passes overhead – yields an observation of a worst case gradient. A small change in any one of these factors can easily lead to missing what would otherwise be a worst-case (i.e., maximum-gradient) data point.

4.0 CONCLUSION

In this paper, we have applied the two-phase method of ionosphere spatial gradient analysis and validation previously developed in [1] to low-elevation satellites on 11/20/03. This method consists of automatic processing of dual-frequency GPS carrier phase measurements of ionosphere delay combined with manual comparison to single-frequency code-carrier divergence measurements to search for an upper bound on anomalous ionosphere gradients.

As a result of this work, we have validated low-elevation spatial gradients in the ionosphere delay at L1 as high as 360 mm/km. These observations were made with CORS network stations in Ohio during the 20 November 2003 ionosphere storm while tracking SVN 26. Station redundancy rules out the possibility of faulty receivers and significant errors in receiver bias estimation. Meanwhile, simultaneous observations on another satellite at a similar elevation, while not as high as 360 mm/km, were anomalously high. Also, observations of ionosphere delay to higher elevation satellites conducted in other studies corroborates that this was a period of very high spatial gradients of at least 300 mm/km at all elevations. Therefore, we conclude that the gradients observed here are not due to a single satellite fault or satellite bias removal error.

Our analysis of other ionosphere data will continue, notably from the 29-31 October 2003 storm, as we continue to refine our estimate of an upper bound on the maximum ionosphere spatial gradients possible at low elevation. From this study, we conclude that very high gradients on the order of 300 mm/km may occur at both high and low elevation angles. We will continue to investigate the possibility of a relationship between the worst-case magnitude of ionosphere gradients and satellite elevation. The impact of these gradients on WAAS precision navigation service is negligible due to the implementation of the WAAS Extreme Storm Detector [9]. We will characterize the impact of large ionosphere gradients on LAAS CAT I availability.

ACKNOWLEDGMENTS

The authors would like to thank Attila Komjathy at Caltech/Jet Propulsion Laboratory for processing the dual-frequency CORS/IGS GPS data and providing it to them. This study was supported by the Federal Aviation Administration (FAA) Local Area Augmentation System (LAAS) Program Office, of whom Carlos Rodriguez, John Warburton, and Barbara Clark were particularly helpful. We would also like to thank Boris Pervan of IIT, Jason Rife of Stanford, and Todd Walter of Stanford for their help and advice.

REFERENCES

1. Ene, A., D. Qiu, M. Luo, S. Pullen, and P. Enge, "A Comprehensive Ionosphere Storm Data Analysis Method to Support LAAS Threat Model Development," Proceedings of ION 2005 National Technical Meeting, San Diego, CA., Jan. 24-26, 2005, pp. 110-130, http://waas.stanford.edu/~wwu/papers/gps/PDF/EneQiuIONNTM05.pdf.

2. Luo, M., S. Pullen, A. Ene, D. Qiu, T. Walter, and P. Enge, "Ionosphere Threat to LAAS: Updated Model, User Impact, and Mitigations," Proceedings of ION GNSS 2004, Long Beach, CA., Sept. 21-24, 2004, pp. 2771-2785, http://waas.stanford.edu/~wwu/papers/gps/PDF/LuoIONGNSS04.pdf.

3. Luo, M., S. Pullen, S. Datta-Barua, G.. Zhang, T. Walter, and P. Enge. "LAAS Study of Slow-Moving Ionosphere Anomalies and Their Potential Impacts," Proceedings of ION GNSS 2005, Long Beach, CA., Sept. 13-16, 2005, pp. 2337-2349, http://waas.stanford.edu/~wwu/papers/gps/PDF/LuoIONGNSS05.pdf.

4. National Geodetic Survey (NGS) - CORS Data and Related Information. URL: http://www.ngs.noaa.gov/CORS/download2/.

5. Lee, J., M. Luo, S, Pullen, Y.S. Park, M. Brenner, and P. Enge, "Position- Domain Geometry Screening to Maximize LAAS Availability in the Presence of Ionosphere Anomalies," Proceedings of ION GNSS 2006, Fort Worth, TX., Sept. 26-29, 2006, http://waas.stanford.edu/~wwu/papers/gps/PDF/LeeIONPLANS06.pdf.

6. FAA/William J Hughes Technical Center, NSTB/WAAS T&E Team, “Wide-Area Augmentation System Performance Analysis Report, Report #7,” 30 Jan 2004. 14 Mar 2005. <ftp://ftp.nstb.tc.faa.gov/pub/archive/REPORTS/waaspan7.pdf>.

7. Foster, J. C., A. J. Coster, P. J. Erickson, F. J. Rich, and B. R. Sandel (2004), Stormtime observations of the flux of plasmaspheric ions to the dayside cusp/magnetopause, Geophys. Res. Lett., 31, L08809, doi:10.1029/2004GL020082.

8. Komjathy, A., L. Sparks, and A.J. Mannucci, "A New Algorithm for Generating High Precision Ionospheric Ground-Truth Measurements for FAA's Wide Area Augmentation System," Jet Propulsion Laboratory, JPL Supertruth Document, Vol. 1, Pasadena, LA, July 2004.

9. Pandya, N., M. Gran, E. Paredes, “WAAS Performance Improvement with a New Undersampled Ionospheric Gradient Threat Model Metric,” Proceedings of ION NTM 2007, San Diego, CA, 22 – 24 January 2007, (in press).